VNU Journal of Science: Mathematics – Physics, Vol. 32, No. 2 (2016) 22-33

Laboratory Measurement of Microstructure Parameters of Porous Rocks

Luong Duy Thanh[1,*], Rudolf Sprik[2]

[1]*Water Resources University, 175 Tay Son, Dong Da, Ha Noi, Vietnam*
[2]*Van der Waals-Zeeman Institute, University of Amsterdam, The Netherlands*

Received 24 April 2016
Revised 24 May 2016; Accepted 24 June 2016

Abstract: Electrokinetic phenomena are induced by the relative motion between a fluid and a solid surface and are directly related to the existence of an electric double layer between the fluid and the solid grain surface. Electrokinetics in porous media plays an important role in geophysical applications and environmental applications. Electrokinetic phenomena depend not only on fluid but also on microstructure parameters of porous media. In order to study the dependence of electrokinetics on microstructure parameters, we have measured the microstructure parameters as well as elastic moduli of 21 porous rock samples including natural rocks and artificial rocks. The experimental results are in good agreement with literature. The results show that there is a big difference in measured parameters between the natural rocks and artificial ones. Namely, the formation factors, the Poisson's ratio of natural rocks are normally higher than those of artificial rocks. However, the porosity, the solid density and the permeability of the natural rocks are smaller than those of the artificial samples. The bulk modulus is normally higher that shear modulus for all samples. Based on the measured parameters, we will study the dependence of electrokinetic coupling coefficient on microstructure parameters of the porous media (in the upcoming paper).

Keywords: Electrokinetics, streaming potential, microstructure parameters, porous media, rocks

1. Introduction

The electrokinetic phenomena are induced by the relative motion between the fluid and the solid surface. In a porous medium such as rocks or soils, the electric current density, linked to the ions within the fluid, is coupled to the fluid flow and that coupling is called electrokinetics e.g. [1]. Electrokinetics consists of several different effects such as streaming potential, seismoelectrics, electroosmosis, electrophoresis etc. Electrokinetics plays an important role in geophysical, environmental, medical applications and others. For example, the streaming potential is used to map subsurface flow and detect subsurface flow patterns in oil reservoirs e.g. [2]. Streaming potential is also used to monitor subsurface flow in geothermal areas and volcanoes [3]. Monitoring of streaming

*Corresponding author. Tel.: 84-936946975
Email: luongduythanh2003@yahoo.com

potential anomalies has been proposed as a means of predicting earthquakes e.g. [4, 5] and detecting of seepage through water retention structures such as dams, dikes, reservoir floors, and canals e.g. [6]. Seismoelectric effects can be used in order to investigate oil and gas reservoirs e.g. [7], hydraulic reservoirs e.g. [8, 9]. Electroosmosis that arises due to the motion of liquid induced by an applied voltage across a porous material or a microchannel is one of the promising technologies for cleaning up low permeable soil in environmental applications. In this process, contaminants are separated by the application of an electric field between two electrodes inserted in the contaminated mass. Therefore, it has been used for the removal of organic contaminants, petroleum hydrocarbons, heavy metals and polar organic contaminants in soils, sludge and sediments e.g. [10, 11].

The coupling coefficient of conversion between electric current density and fluid flow depends not only on fluid (ionic species present in the fluid, pH, fluid composition, fluid electrical conductivity and temperature) but also on microstructure parameters of porous media (porosity, density of grains, tortuosity, formation factor and steady-state permeability). In previously published work, we have studied the dependence of streaming potential coupling coefficient on permeability of porous media. The results have shown that the streaming potential coupling coefficients strongly depend on the permeability of the samples for low fluid conductivity. When the fluid conductivity is larger than a certain value, the streaming potential coupling coefficient is independent of permeability [12].

In this work, we briefly introduce the definition of the microstructure parameters of porous media. The approaches and experimental setups to measure those parameters are then presented. In addition, the frame and shear modulus of the porous media that characterize elastic properties of the porous media are also measured. Measurements have been carried out for 21 rock samples. The experimental results show that there is a big difference in measured parameters between the natural rocks and artificial ones. Namely, the formation factors, the Poisson's ratio of natural rocks are always higher than those of artificial ones. However, the porosity, the solid density and the permeability of the natural rocks are smaller than those of the artificial samples. The compressional wave velocity is greater than that of shear wave velocity. The bulk modulus is normally higher that shear modulus for all samples. Based on the measured parameters, we will study the dependence of streaming potential coupling coefficient on porosity, density of grains, tortuosity, formation factor, the frame and shear modulus of the porous media (in the upcoming paper).

This work has four sections. In the first we briefly introduce definitions of microstructure parameters of porous media. In the second we present the experimental measurements. The third section contains the experimental results and discussion. Conclusions are provided in the final section.

2. Microstructure parameters of porous media

In this section, we briefly introduce definitions of microstructure parameters of porous media such as the porosity, permeability, solid density, tortuosity and formation factor.

2.1. Porosity

Porosity is a measure of the void spaces in a porous material, and is a fraction of the volume of voids over the total volume, between 0 and 1, or as a percentage between 0 and 100 % (see Figure 1 on the left side). It is given by

$$\varphi = \frac{V_p}{V_b}, \qquad (1)$$

where V_p is the pore volume (volume of void space) and V_b is the bulk volume of the material (total volume) including the solid and void spaces (see [13] for more details).

2.2. Permeability

Permeability is a measure of the ability of a porous material to allow fluids to pass through it. High permeability will allow fluids and gases to move rapidly through the porous materials and vice versa. Permeability depends on the connected voids within the porous materials and on the size, shape, and arrangement of the connected pores [13]. The SI unit for permeability is m^2. A practical unit for permeability is the Darcy (D), or more commonly the miliDarcy - mD (1 Darcy $\approx 10^{-12}$ m^2).

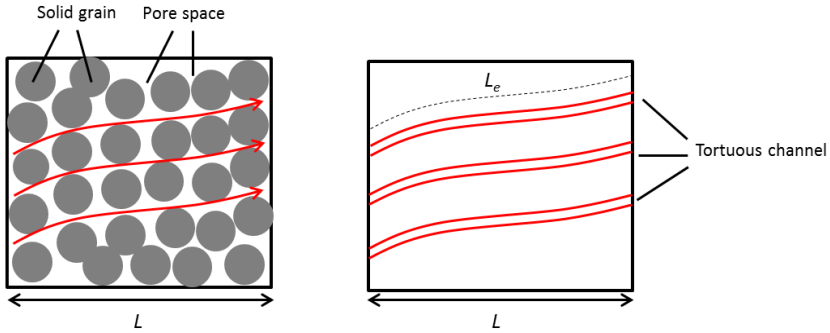

Figure 1. Schematic of a porous medium model with idealized cylindrical channels of uniform diameter.

2.3. Solid density

The solid density or particle density is the density of the particles (solid grains) that make up porous materials (see Figure 1 on the left side), in contrast to the bulk density, which measures the average density of a large volume of the materials. The solid density is defined as follows

$$\rho_s = \frac{m_s}{V_s}, \qquad (2)$$

where m_s is the solid phase mass and V_s is the volume of the solid phase of the porous materials.

2.4. Tortuosity and formation factor

The actual fluid velocity, v_a, within the pores (channels) of a porous medium is greater than the macroscopic velocity, v, implied by Q_f/A (Q_f is the volumetric flow rate and A is the cross sectional area of the porous medium). The increase of velocity is partially a result of the increase of the actual flow path length, L_e, compared to the theoretical bulk length of the porous medium, L (see Figure 1). The actual fluid velocity is given by (see [14] for more details)

$$v_a = \frac{v}{\varphi}\frac{L_e}{L} = \frac{v}{\varphi}\alpha_\infty, \qquad (3)$$

where ϕ is the porosity mentioned above, $\alpha_\infty = L_e/L$ is defined as the tortuosity of the porous medium (the ratio of actual passage length to the theoretical bulk length of the porous medium) and the ratio of α_∞/ϕ is defined as the formation factor of the porous medium and usually denoted as F [15].

3. Experiment

Table 1. Sample ID, mineral compositions and microstructure parameters of the samples. Symbols k_o (in mD), ϕ (in %) , F (no units), α_∞ (no units), ρ_s (in kg/m^3) stand for permeability, porosity, formation factor, tortuosity and solid density of porous media, respectively. For lithology, EST stands for Estaillade limestone, IND stands for Indiana Limestone, BER and BereaUS stand for Berea sandstone, BEN stands for Bentheim sandstone, and DP stands for artificial ceramic core.

	Sample ID	Mineral compositions	k_o	ϕ	F	α_∞	ρ_s
1	BereaUS1	Silica, Alumina, Ferric Oxide, Ferrous Oxide (www.bereasandstonecores.com)	120	14.5	19.0	2.8	2602
2	BereaUS2	-	88	15.4	17.2	2.6	2576
3	BereaUS3	-	22	14.8	21.0	3.1	2711
4	BereaUS4	-	236	19.1	14.4	2.7	2617
5	BereaUS5	-	310	20.1	14.5	2.9	2514
6	BereaUS6	-	442	16.5	18.3	3.0	2541
7	DP50	Alumina and fused silica (see: www.tech-ceramics.co.uk)	2960	48.5	4.2	2.0	3546
8	DP46i	-	4591	48.0	4.7	2.3	3559
9	DP217	-	370	45.4	4.5	2.0	3652
10	DP215	-	430	44.1	5.0	2.0	3453
11	DP43	-	4753	42.1	5.5	2.3	3370
12	DP172	-	5930	40.2	7.5	3.0	3258
13	DP82/81		47	44.1	5.0	2.1	3445
14	EST	Mostly Calcite (see[16])	294	31.5	9.0	2.8	2705
15	IND01	Mostly Calcite, Silica, Alumina, Magnesium carbonate (see [17, 18])	103	20.0	32.0	6.4	2745
16	BER5	Silica (74.0-98.0%), Alumina and clays (see [29, 30])	51	21.1	14.5	3.1	2726
17	BER12		48	22.9	14.0	3.2	2775
18	BER502	-	182	22.5	13.5	3.0	2723
19	BER11		740	24.1	14.0	3.4	2679
20	BEN6	Mostly Silica (see [31])	1382	22.3	12.0	2.7	2638
21	BEN7	Mostly Silica (see [31])	1438	22.2	12.6	2.8	2647

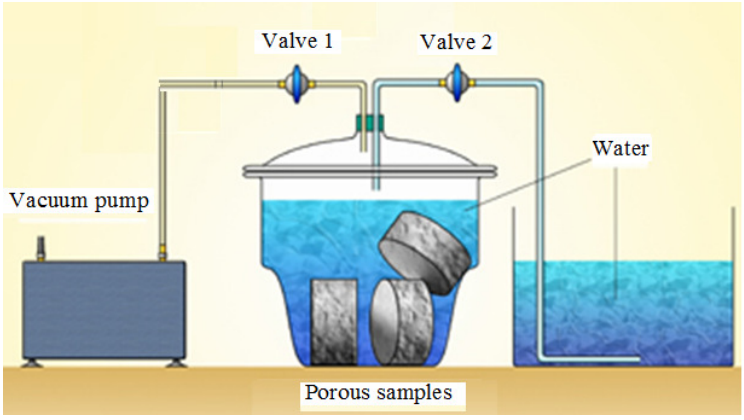

Figure 2. Schematic of the experimental setup for porosity measurement.

In this section, the approaches and experimental setups to measure microstructure parameters as well as the frame and shear modulus of porous media are presented. The porous media used for the measurement are 21 cylindrical rock samples (55 mm in length and 25 mm in diameter) from different sources. The natural samples numbered from 1 to 6 were obtained from Berea Sandstone Petroleum Cores Company in the US. Artificial samples numbered from 7 to 13 were obtained from HP Technical Ceramics company in England. The natural samples numbered from 14 to 20 were obtained from Shell oil company in the Netherlands. The last one numbered 21 was obtained from Delft University in the Netherlands. The mineral composition of all samples is shown in Table 1.

3.1. Porosity

The porosity is measured by a simple method [21]: The sample is first dried in oven for 24 hours, cooled to room temperature and fully saturated with deionized water under vacuum as shown in Figure 2. The sample is weighed before (m_{dry}) and after saturation (m_{wet}), and the porosity is determined as:

$$\varphi = \frac{(m_{wet} - m_{dry})/\rho}{AL}, \qquad (4)$$

where ρ is density of the water, A and L are the cross sectional area and the physical length of the samples, respectively.

3.2. Solid density

The solid density ρ_s is determined from

$$\rho_S = \frac{m_{dry}}{(1-\varphi)AL} \qquad (5)$$

3.3. Permeability

Permeability is determined by a constant flow-rate experiment as shown in Figure 3. A high pressure pump (LabHut, Series III- Pump) ensures a constant flow through the sample, a high precision differential pressure transducer (Endress and Hauser Deltabar S PMD75) is used to measure the pressure drop. For low velocities Darcy's law holds

$$Q_f = -\frac{k_o A}{\eta}\frac{\Delta P}{L}, \qquad (6)$$

where Q_f is the fluid volume flow rate, k_o is the permeability, ΔP is the differential pressure imposed across the sample, η is the viscosity of the fluid. The permeability is then determined from the slope of the flow rate - pressure graph as shown in Figure 8.

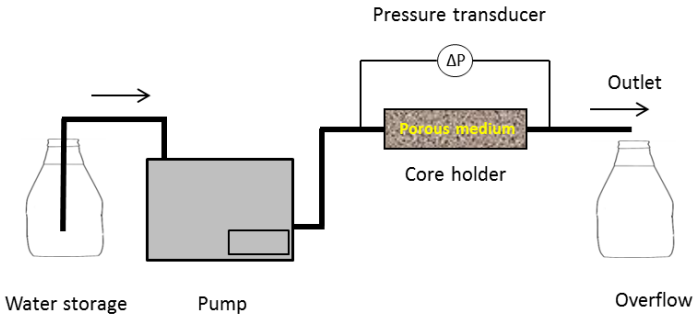

Figure 3. Schematic of the experimental setup for permeability measurement.

3.4. Tortuosity

Method of determining the tortuosity was proposed in [22]. They defined the formation factor F as:

$$F = \frac{\alpha_\infty}{\varphi} = \frac{\sigma_f}{\sigma_r}, \qquad (7)$$

where α_∞ is the tortuosity, σ_r is the electrical conductivity of the saturated sample, σ_f is the electrical conductivity of the fluid and ϕ is the porosity of the sample. Schematic of the experimental setup to measure the tortuosity and formation factor is shown in Figure 4. A cylindrical porous sample is jacketed in a tight (nonconducting) silicon sleeve. The electrodes for the resistivity measurements are silver membrane filters (Cole-Parmer). They are thin and very permeable so that they do not affect the permeability of the porous sample. The membrane electrodes are placed on both sides against the porous sample that is saturated successively with a set of aqueous NaCl solutions with high conductivities. Eq. 7 is valid when surface conductivity effects become negligible (at high fluid electric conductivities, σ_f). Frequency-dependent porous sample resistance is measured directly by an impedance analyzer (Hioki IM3570) after saturation to calculate σ_r with the knowledge of the geometry of the sample (the length, the diameter). A conductivity measurement by the conductivity meter (Consort C861) in the solution containers directly gives σ_f.

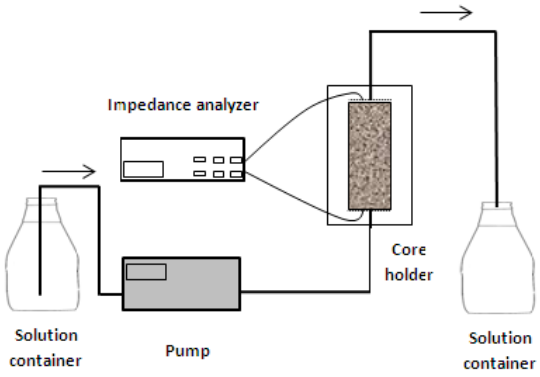

Figure 4. Experimental setup for tortuosity measurement of consolidated samples.

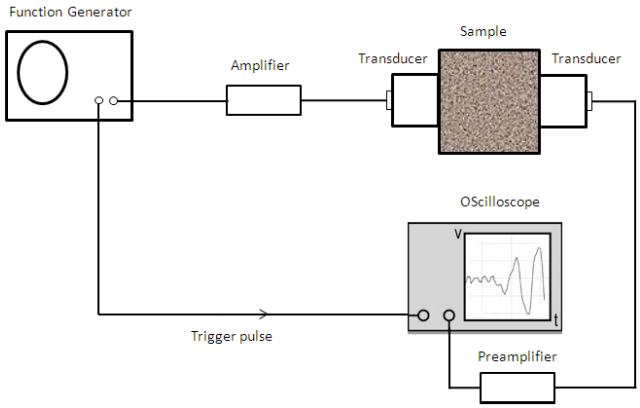

Figure 5. Schematic of the ultrasonic setup for measurement of frame and shear modulus.

3.5. Frame and shear modulus

The (fast) compressional and shear wave speeds, respectively v_P and v_S, of air saturated porous samples are related to the frame modulus K_P and shear modulus G_S as follows [23]:

$$v_P = \sqrt{\frac{K_P + \frac{4}{3}G_S}{(1-\varphi)\rho_s}}, \quad (8)$$

$$v_S = \sqrt{\frac{G_S}{(1-\varphi)\rho_s}}, \quad (9)$$

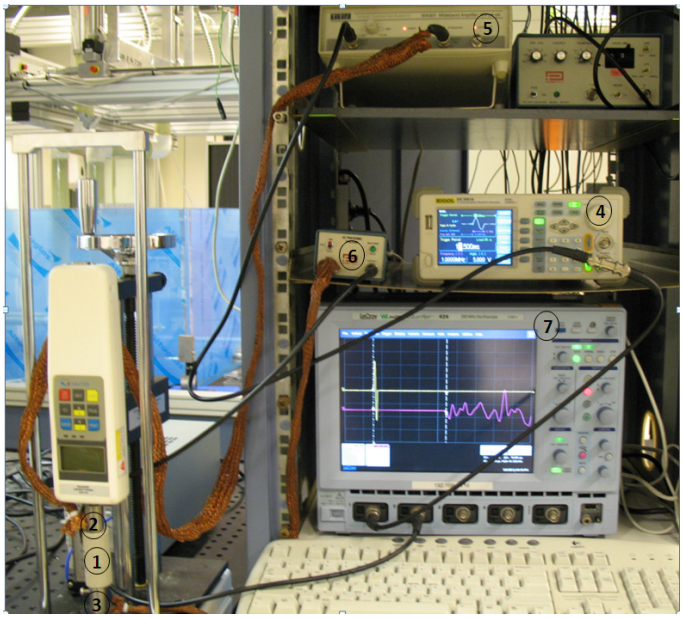

Figure 6. Photo of the ultrasonic setup. A sample (1) is clamped between two identical P-wave transducers (2) and (3). The sending transducer is connected to the function generator (4) through the voltage amplifier (5), while the receiving transducer is connected to the oscilloscope (7) through the preamplifier (6).

Dry compressional and shear wave measurements are performed at room conditions using a standard pulse transmission bench-top set-up as shown in Figure 5 and Figure 6. The experimental set-up to measure velocity consists of a function generator (Rigol model DG3061A), an oscilloscope (Lecroy Wavesurfer 424), an amplifier (TTI Wideband Amplifier WA-301) and a preamplifier (Panametrics 5670). Molasses is used to enhance the transducer-sample coupling. Two transducer pairs with a flat element diameter (Panametrics-PZT V133 and V153) allow measurements of the compressional and shear wave velocity at frequency of 1.0 MHz. The system delay is calibrated by face-to-face measurements of the transducers and is designated as t_c. The wave velocity is calculated from tip to tip distance (the length of the sample) between the two transducers (L) and the time to cover this distance as below:

$$v = \frac{L}{t - t_c}, \quad (10)$$

where v is the wave velocity and t is the total travel time read from Figure 7 for the sample BereaUS5, for example. Poisson's ratio is related to compressional wave velocity (v_P) and shear wave velocity (v_S) by [24]

$$\gamma = \frac{(v_P^2 - 2v_S^2)}{2((v_P^2 - v_S^2)}, \quad (11)$$

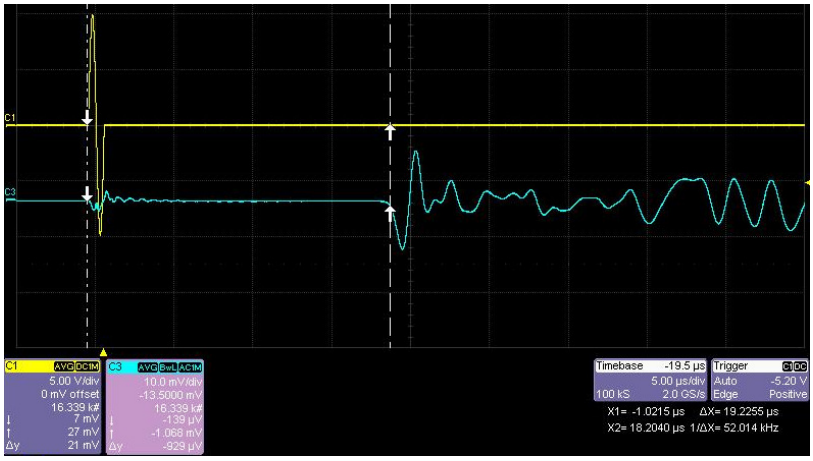

Figure 7. Compressional wave result for BereaUS5.

4. Results and discussion

Porosity and density of the samples are shown in Table 1 with an error of 3% and of 5%, respectively. The measured porosities vary from 14.5% (BereaUS1) to 48.5% (DP50). Porosity of natural rocks is higher than that of artificial rocks (around two times). The density of the solid grains lies between 2576 kg/m^3 (BereaUS2) and 3652 kg/m^3 (DP217). The solid density of artificial rocks is higher than that of natural rocks. The solid density of sandstone rocks (Berea and Bentheim sandstone) is close to that of silica particles (2650 kg/m^3) and is in good agreement with values reported in [23]. That is reasonable because sandstone rocks are mainly made up of silica. It should be noted that the parameters reported in Table 1 have been partially reported in [25] without any details about the experimental setup and approaches.

Figure 8 shows a representative graph of flow rate as a function of applied pressure difference for the sample BereaUS5. The graph shows that there is a linear relationship between flow rate and pressure difference and Darcy's law is obeyed as expected from the maximum Reynolds number of 0.05 for our measurements. That value is much smaller than the critical maximum value, Re = 1 below which fluid flows are creeping flows (for more details, see [26]). It should be note that the Reynolds number is defined as

$$\mathrm{Re} = \frac{\rho v l}{\eta}, \quad (12)$$

where ρ is the fluid density, v is the fluid velocity, l is a characteristic length of fluid flow determined by pore dimensions and η is the fluid viscosity. For our measurements, ρ is taken as 10^3 kg/m^3, v is 10^{-3} m/s, l is 5×10^{-5} m and η is 10^{-3} Pa.s. From the slope of the graph and Darcy's law, the

permeability of the sample is obtained. The permeability of all samples is reported in Table 1 with an error of 5%. The results show that the permeability of the natural rocks is much smaller than that of the artificial samples.

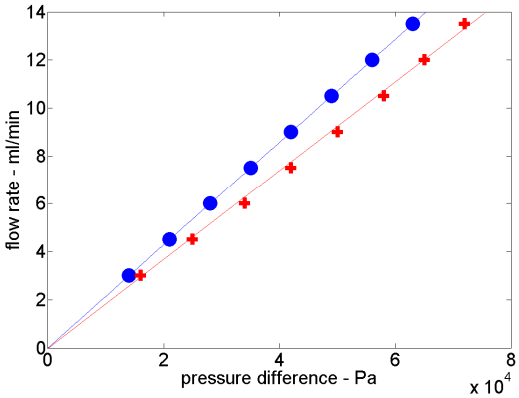

Figure 8. The flow rate against pressure difference. Two runs are shown for the sample BereaUS5.

An example of the electrical conductivity of the samples (σ_r) versus the electrical conductivity of the electrolyte (σ_f) is shown in Figure 9 for the sample BereasUS5. The formation factor as the reciprocal of the slope of a linear regression through the data points is obtained. It is seen that the linear part of the curve shown in Figure 9 approximately starts from the value of fluid electric conductivity of 0.50 S/m. Values of the formation factor and corresponding tortuosity for all samples are also reported in Table 1 with an error of 6 % and 9 %, respectively. The experimental results show that the formation factor of the natural rocks is always higher than that of the artificial samples.

Based on Table 1, formation factor of the samples as a function of porosity is plotted in Figure 10. According to Archie's law, we have $F = \phi^{-m}$ (F is the formation factor, ϕ is the porosity of the sample and m is the so-called cementation exponent). The value of m varies mainly with pore geometry and the degree of consolidation of the rock. The cementation exponent m lies from 1.14 to 2.52 and it can reach 2.9 or higher for carbonate formations [14]. Figure 10 is in good agreement with Archie's law with m of 1.5 (the fitting line) except the data point for sample IND01 (the point far from the fitting line). The reason may be that the sample IND01 is mainly made of carbonate (calcite).

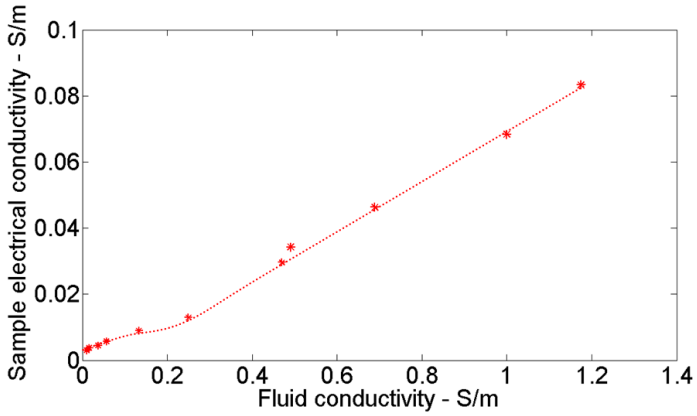

Figure 9. Electrical conductivity of the sample versus fluid electric conductivity for the sample BereaUS5. The dash line is used to show a linear part.

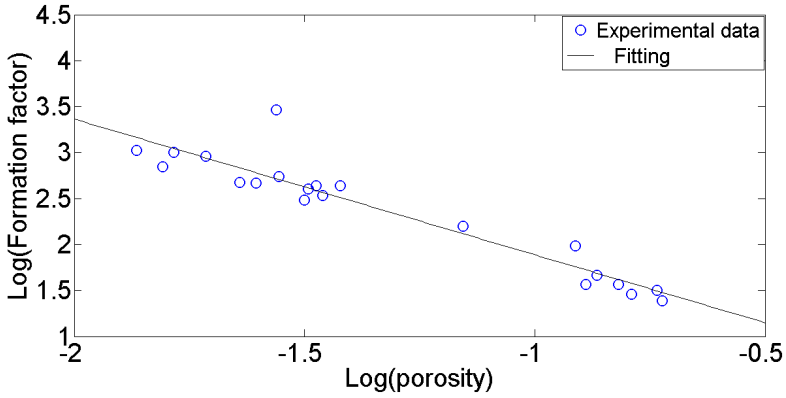

Figure 10. Formation factor versus porosity.

Before carrying out velocity measurement for the samples, we do the velocity calibration by using aluminum and brass blocks of different lengths. The compressional and shear wave velocities for the reference solids are in agreement with the values from literature, as shown in table 2.

Table 2. Measured material properties of reference solids compared to their literature values. The density ρ_s and compressional and shear wave velocities v_P and v_S are measured using the conventional techniques discussed in the text. The literature values are from [24, 27].

Solid	Measured values			Literature values		
	v_P [m/s]	v_S [m/s]	density	v_P [m/s]	v_S [m/s]	density
Aluminum	6292	3195	2710	6250-6500	3040-3130	2700
Brass	4295	1982	8449	4280-4440	2030-2120	8560

Table 3. Measured parameters of the samples. In which v_P, v_S, K_P, G_S and γ are compressional velocity, shear velocity, bulk modulus, shear modulus and Poisson's ratio, respectively.

	Sample ID	v_P [m/s]	v_S [m/s]	K_P [GPa]	G_S [GPa]	γ
1	BereaUS1	2928	1767	9.67	6.86	0.21
2	BereaUS2	3018	1725	11.15	6.46	0.26
3	BereaUS3	2913	1749	10.09	7.00	0.22
4	BereaUS4	2758	1498	9.65	4.69	0.29
5	BereaUS5	2819	1506	10.14	4.67	0.30
6	BereaUS6	3200	1667	13.75	5.85	0.31
7	DP50	2782	1808	6.13	5.92	0.13
8	DP46i	3059	1921	8.26	6.86	0.17
9	DP217	3605	2304	12.33	9.40	0.18
10	DP215	3505	2204	11.33	9.48	0.17
11	DP43	2956	1796	8.78	6.39	0.20
12	DP172	3430	2270	9.62	10.14	0.11
13	DP82/81	3570	2340	9.75	10.23	0.12
14	EST	3009	1829	8.58	6.16	0.21

15	IND01	3784	2100	18.52	9.68	0.28
16	BER5	3031	1647	11.95	5.83	0.29
17	BER12	2968	1699	10.61	6.17	0.26
18	BER502	2765	1594	9.00	5.37	0.25
19	BER11	2660	1316	9.66	3.51	0.34
20	BEN6	2849	1464	10.76	4.39	0.32
21	BEN7	2898	1509	11.02	4.68	0.31

The compressional and shear wave velocities are obtained for all samples and shown in Table 3. The error in the velocity measurements is estimated to be 3%. The elastic moduli are calculated from the dry velocities using eqs (8) and (9) and shown in Table 3. In the Table we observe that $v_P > v_S$ for all samples, while $K_P > G_S$ for about 90 % of the samples. Similar percentages have been reported by [23, 28]. In general, high v_P/v_S ratios correspond to unconsolidated sediments, while medium and low v_P/v_S ratios correspond to dry consolidated sediments [29]. Poissons ratio is calculated using eqs (11) and shown in Table 3. Poisson's ratio values for the samples lie between 0.11 (DP172) and 0.34 (BER11) and are in good agreement with those of rocks reported in [30]. The experimental results show that the Poisson's ratio of the natural rocks is greater than that of the artificial ones.

5. Conclusions

In this work, we briefly introduce the definition of the microstructure parameters of porous media that are very important in the electrokinetic phenomena. The approaches and experimental setups to measure those parameters are then presented. In addition, the frame and shear modulus of the porous media that characterize elastic properties of the porous media are also measured. Measurements have been carried out for 21 samples including both natural and artificial rocks. The experimental results are in good agreement with those reported in literature. Therefore, the validity of the measurements has been checked.

The experimental results show that there is a big difference in the measured parameters between the natural rocks and artificial ones. Namely, the formation factors, the Poisson's ratio of natural rocks are higher than those of artificial rocks. However, the porosity, the solid density and the permeability of the natural rocks are smaller than those of the artificial samples. The reasons for the difference in microstructure parameters between the natural rocks and the artificial ones are probably the differences in mineral composition (one is mainly made of silica and the other is mainly made of alumina) and in the conditions in which the rocks are formed (pressure, temperature etc). The compressional wave velocity is greater than that of shear wave velocity. The bulk modulus is normally higher that shear modulus for all samples. This work has also added to the existing experimental data of the microstructure parameters as well as elastic moduli for various types of rock that is very important in electrokinetics. Based on the measured parameters, we will study the dependence of streaming potential coupling coefficient on porosity, density of grains, tortuosity, formation factor, the frame and shear modulus of the porous media (in the upcoming paper).

Acknowledgments

This work has been carried out at the Van der Waals-Zeeman Institute/Institute of Physics, University of Amsterdam.

References

[1] L. Jouniaux, T. Ishido, International Journal of Geophysics (2012).

[2] B. Wurmstich, F. D. Morgan, Geophysics 59 (1994) 46–56.

[3] R. F. Corwin, D. B. Hoovert, Geophysics 44 (1979) 226–245.

[4] H. Mizutani, T. Ishido, T. Yokokura, S. Ohnishi, Geophys. Res. Lett. 3 (1976).

[5] M. Trique, P. Richon, F. Perrier, J. P. Avouac, J. C. Sabroux, Nature (1999) 137–141.

[6] A. A. Ogilvy, M. A. Ayed, V. A. Bogoslovsky, Geophysical Prospecting 17 (1969) 36–62.

[7] A. Thompson, S. Hornbostel, J. Burns, et al., SEG Technical Program Expanded Abstracts (2005).

[8] S. Haines, A. Guitton, B. Biondi, Geophysics 72 (2007) G1–G8.

[9] S. Garambois, M. Dietrich, Geophysics 66 (2001) 1417–1430.

[10] T. Paillat, E. Moreau, P.O.Grimaud, G. Touchard, IEEE Transactions on Dielectrics and Electrical Insulation 7 (2000) 693–704.

[11] C. Cameselle, S. Gouveia, D. E. Akretche, B. Belhadj, Organic Pollutants - Monitoring, Risk and Treatment, InTech, 2013.

[12] L. D. Thanh, R. Sprik, Geophysical Prospecting, DOI: 10.1111/13652478.12337 (2015).

[13] R. B. Robert, Reservoir Sandstones, Prentice Hall College Div, 1985.

[14] Z. Bassiouni, Theory, Measurement, and Interpretation of Well Logs, Henry L. Doherty Memorial Fund of AIME, Society of Petroleum Engineers, 1994.

[15] A. Y. Dandekar, Petroleum Reservoir Rock and Fluid Properties, CRC Press, 2013.

[16] E. Bemer, O. Vincke, P. Longuemare, Oil and Gas Science and Technology 59 (2004) 405–426.

[17] I. T. Committee, Indiana Limestone Handbook, Indiana Limestone Institute of America, Inc., 2007.

[18] P. Churcher, P. French, J. Shaw, L. Schramm, SPE International Symposium (1991).

[19] A. Pagoulatos, Evaluation of multistage Triaxial Testing on Berea sandstone, Degree of Master of Science, Oklahoma, 2004.

[20] A. A. Tchistiakov, Proceedings World Geothermal Congress (2000).

[21] S. Zeng, C. H. Chen, J. C. Mikkelsen, J. G. Santiago, Sens. Actuators B 79 (2001) 107–114.

[22] R. Brown, Geophysics 45 (1980) 1269–1275.

[23] C. Wisse, On frequency dependence of acoustic waves in porous cylinders, Ph.D. thesis, Delft University of Technology, the Netherlands, 1999.

[24] A. Kumar, T. Jayakumar, B. Raj, K. Ray, Acta Materialia 51 (2003) 2417–2426.

[25] D. T. Luong and R. Sprik, International Journal of Geophysics, Article ID 471819, doi:10.1155/2014/471819 (2014).

[26] G. Mavko, T. Mukerj, J. Dvorkin, The Rock Physics Handbook - Tools for Seismic Analysis in Porous Media, Cambridge University Press, 2003.

[27] T. Kundu, Ultrasonic Nondestructive Evaluation: Engineering and Biological Material Characterization, CRC Press, New York, USA, 2003.

[28] B. Vogelaar, Fluid effect on wave propagation in heterogeneous porous media, Ph.D. thesis, Delft University of Technology, the Netherlands, 2009.

[29] T. Bourbie, O. Coussy, B. Zinszner, Acoustics of Porous media, Institut Francais du Petrole Publications, Gulf Publishing Company, 1987.

[30] T. B. Odumosu, C. Torres-Verdin, J. M. Salazar, J. Ma, B. Voss, G. L. Wang, Society of Petroleum Engineers (2009).